square vessel would also generate antivortices in order to comply with the imposed symmetry. By proper arrangement of the laser fields, the vortex patterns in Bose–Einstein condensates confined by triangular or square traps could also reveal symmetry-induced antivortices.

Our symmetry-conserving results for a triangle form a natural generalization to superconducting boundary conditions of the quantum-mechanical problem of a "particle in an equilateral triangle"[14]. An intriguing correspondence can be drawn between the eigenstates in the triangle and families of leptons (electrons or muons) and quarks. □

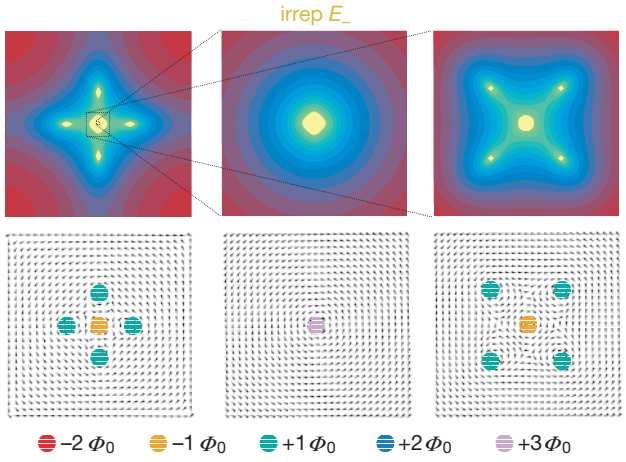

Figure 4 Vortex entry into a square for applied magnetic fields generating three flux quanta. The symmetry of the corresponding states is E_- (dark yellow curves in Fig. 1). The same colour conventions as in Fig. 2 were used. The central region of the square is magnified 64 times, for the middle plots, and 8 times for the plots on the right. In this mode, the lateral Φ_0-vortices approach and merge with the central antivortex to form a giant $3\Phi_0$-vortex. With increasing field, the $3\Phi_0$-vortex will split into four diagonal Φ_0-vortices and the initial single antivortex (on the right). In order to be able to see the four separate Φ_0-vortices, the panels on the right had to be magnified. This is owing to the strong attraction of the Φ_0-vortices to the central antivortex. For the same reason, the spacing between the three dark yellow squares in Fig. 1a is large, as compared to the other irreps.

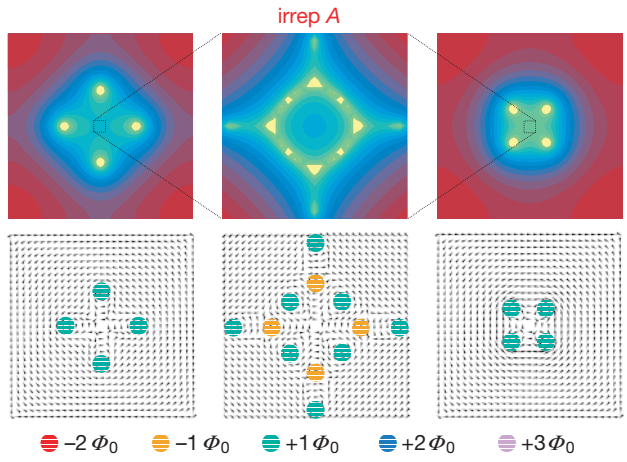

Figure 5 Vortex entry into a square for applied magnetic fields generating four flux quanta. The symmetry of the corresponding states is A (red curves in Fig. 1). The same colour conventions as in Fig. 2 were used. The middle plots correspond to the central region of the square magnified 16 times. In the initial stage (left), there is no central vortex in this case. The approach of the lateral Φ_0-vortices induces the creation of a central vortex–antivortex pattern (central panels), which is however rotated by 45°, as compared to Fig. 2. At higher flux (on the right), the lateral vortices and antivortices will annihilate, leaving four diagonal Φ_0-vortices which move towards the corners.

1. Moshchalkov, V. V. *et al.* in *Handbook of Nanostructured Materials and Nanotechnology* (ed. Nalwa, H. S.) Vol. 3, Ch. 9, 451–525 (Academic, San Diego, 1999).
2. de Gennes, P.-G. *Superconductivity of Metals and Alloys* (Benjamin, New York, 1966).
3. Saint-James, D. & de Gennes, P.-G. Onset of superconductivity in decreasing fields. *Phys. Lett.* **7,** 306–308 (1963).
4. Landau, L. D. & Lifshitz, E M. *Quantum Mechanics* 2nd edn (Pergamon, Oxford, 1975).
5. Bruyndoncx, V., Strunk, C., Moshchalkov, V. V., Van Haesendonck, C. & Bruynseraede, Y. Fluxoid quantization effects in superconducting mesoscopic Al multiloop structures. *Europhys. Lett.* **36,** 449–454 (1996).
6. Saint-James, D. Etude du champ critique H_{c3} dans une géometrie cylindrique. *Phys. Lett.* **15,** 13–15 (1965).
7. Abrikosov, A. A. *Fundamentals of the Theory of Metals* (North-Holland, Amsterdam, 1988).
8. Chang, A. M. *et al.* Scanning Hall probe microscopy. *Appl. Phys. Lett.* **61,** 1974–1976 (1992).
9. Oral, A., Bending, S. J. & Henini, M. Real-time scanning Hall probe microscopy. *Appl. Phys. Lett.* **69,** 1324–1326 (1996).
10. Hess, H. F., Robinson, R. B., Dynes, R. C., Valles, J. M. Jr & Waszcak, J. V. Scanning-tunneling-microscope observation of the Abrikosov flux lattice and the density of states near and inside a fluxoid. *Phys. Rev. Lett.* **62,** 214–216 (1989).
11. Maggio-Aprile, I., Renner, Ch., Erb, A., Walker, E. & Fischer, O. Direct vortex lattice imaging and tunneling spectroscopy of flux lines on $YBa_2Cu_3O_{7-\delta}$. *Phys. Rev. Lett.* **75,** 2754–2757 (1995).
12. Moser, A. *et al.* Observation of single vortices condensed into a vortex-glass phase by magnetic force microscopy. *Phys. Rev. Lett.* **74,** 1847–1850 (1995).
13. Harada, K. *et al.* Direct observation of vortex dynamics in superconducting films with regular arrays of defects. *Science* **274,** 1167–1169 (1996).
14. Li, W.-K. & Blinder, S. M. Solution of the Schrödinger equation for a particle in an equilateral triangle. *J. Math. Phys.* **26,** 2784–2786 (1985).

Acknowledgements

The work was supported by the ESF programme VORTEX, Concerted Action Scheme (GOA) of the Flemish Government and by the Fonds voor Wetenschappelijk Onderzoek Vlaanderen (FWO). We would like to thank L. Van Look for taking the atomic force microscope micrograph.

Correspondence and requests for materials should be addressed to V.V.M. (e-mail: victor.moshchalkov@fys.kuleuven.ac.be).

Flexible filaments in a flowing soap film as a model for one-dimensional flags in a two-dimensional wind

Jun Zhang*†, Stephen Childress*, Albert Libchaber† & Michael Shelley*

* *Applied Mathematics Laboratory, Courant Institute, New York University, New York 10012, USA*
† *Center for Studies in Physics and Biology, Rockefeller University, New York 10021, USA*

The dynamics of swimming fish and flapping flags involves a complicated interaction of their deformable shapes with the surrounding fluid flow. Even in the passive case of a flag, the flag exerts forces on the fluid through its own inertia and elastic responses, and is likewise acted on by hydrodynamic pressure and drag. But such couplings are not well understood. Here we study these interactions experimentally, using an analogous system of flexible filaments in flowing soap films. We find that, for a single filament (or 'flag') held at its upstream end and otherwise unconstrained, there are two distinct, stable dynamical states. The first is a stretched-straight state: the filament is immobile and aligned in the flow direction. The existence of this state seems to refute the common belief that a flag is always unstable and will flap[1,2]. The second is a flapping state: the filament executes a sinuous motion in a manner akin to the flapping of a flag in the wind. We study further the hydrodynamically coupled interaction between two such filaments, and demonstrate the existence of four different dynamical states.

Experiments that cleanly reveal the nature of interactions between a deformable body and a flow are difficult to perform, with complications including the control of three-dimensional flow effects and the challenge of flow visualization. Soap film is a convenient experimental system that resembles two-dimensional hydrodynamics in many respects[3–7]. In this experiment, we take advantage of the relative simplicity of this system, and use the flowing soap film as a laminar two-dimensional flow tunnel. The experimental set-up is shown in Fig. 1. The horizontal span of the tunnel is 8.5 cm, the typical film thickness 3–4 μm, and flow speeds 200–300 cm s^{-1} (see Methods). The experiment is performed 80 cm below the flow entrance, at the midline. The filaments are 0.15 mm in diameter and 2–6 cm long. Their linear density is about 2.0×10^{-4} g cm^{-1}. The rigidity of the filament is estimated to be the order of 0.1 erg cm, tested in a steady soap film where the deflection is measured under a known force. The fluid wets the filament, with surface tension forces constraining the filament to lie always in the plane of the film. The length of the filament can be changed incrementally through the holder at the upstream end, which abuts the film perpendicularly.

At a fixed flow rate, there exists a critical filament length L_c, below which the filament is stretched straight and aligned with the flow. Regardless of the magnitude of an externally imposed disturbance, after a few oscillations, the filament quickly returns to this rest state. If, however, the length of the filament exceeds L_c, the system becomes bi-stable, and two different stable dynamical states are observed. One remains the stretched-straight state, as when $L < L_c$. Figure 2a shows such a state (exposure time 0.5 ms). Using a monochromatic light source, the photograph shows instantaneous interference patterns that reveal small thickness variations. A narrow von Kármán vortex 'street'[8,9] (that is, a train of vortices of alternating signs) can be seen trailing behind the filament. We note that this street is shed starting from the free end rather than from the top, where the flow first encounters the filament. Despite the oscillations of the street, the filament remains a static, seemingly rigid body. Indeed, transient small disturbances (such as a small displacement at the free end, or a thin vortex wake produced by a cylinder placed upstream) do not destroy the stability of this state.

However, if the external perturbation is sufficiently large, the filament jumps to a stable flapping state (Fig. 2b), whose persistence is quite robust to perturbation. Unlike a simple pendulum, the undulation is well fitted by a travelling harmonic wave with a spatially varying envelope:

$$y(x, t) = f(x)\sin(2\pi\nu t + 2\pi x/\lambda)$$

Here, $y(x, t)$ is the horizontal displacement of the filament from the centre-line, measured at a vertical distance x from the fixed point for time t. $f(x)$ is a spatial envelope function (increasing monotonically from the fixed point), ν is the flapping frequency and λ the wavelength. When the filament length is about 3 cm long and flow speed 280 cm s^{-1} (the corresponding Reynolds number is of the order of 10^4), we observed a typical flapping frequency of about 50 Hz and an amplitude (the total excursion of the free end) of about 1.5 cm. A thin vortex street is still evident, but is strongly modified by the large-scale flapping motion. The successive small eddies produced by a single stroke are now of a single sign, unlike the alternating signs in the stretched-straight case. This local vortex

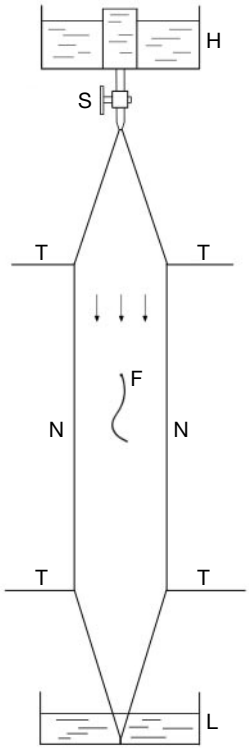

Figure 1 Experimental set-up. A vertical soap film is fed from the top (H) with a solution of 1.5% Dawn, a commercial brand of dishwashing liquid soap, in distilled water. The pressure head is fixed using an overflow mechanism. The attached nozzle (S) regulates the flux. Two nylon threads under tension (T), spread from the nozzle, run parallel, and then converge into the receiving container (L). The upper end of the silk filament (F) is fixed using a thin tube, which is introduced normal to the film plane.

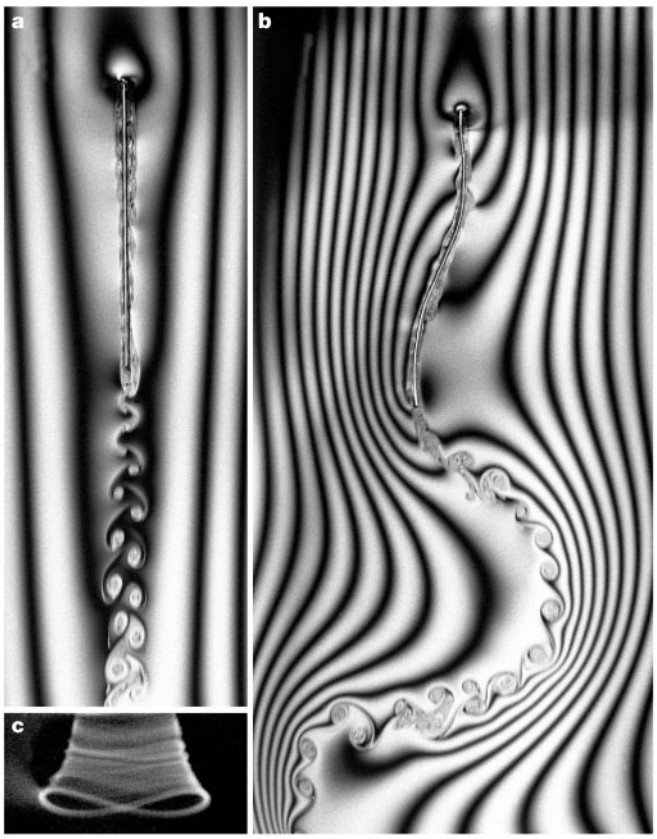

Figure 2 The two stable states of the filament. When the filament length is greater than the critical value, it can stay in either a stretched-straight state or an oscillatory state. The flow is visualized using interference patterns under a sodium lamp. **a**, The filament is stretched straight in the flow. Von Kármán type vortices are shed from its free end. **b**, The oscillatory flapping state. Flow structures, modulated by the filament, are advected downstream. Interference fringes run in the flow direction, indicating that the soap film is under little stretching and compression. **c**, The free end of the filament shows a 'figure of eight' trajectory owing to the existence of the travelling waves associated with the flapping motion.

structure resembles that resulting from a Kelvin–Helmholtz instability[10], suggesting that each stroke and counter-stroke produces a shear-layer of alternating sign. The resulting vortical field does not develop eddies of a size comparable to the flapping amplitude. This is significantly different from a von Kármán street behind a cylinder, or the wake generated by the tail of a flapping fish (ref 11 and ref. 12 and references therein), where one observes vortices of a size comparable to the body. In Fig. 2c, the lower part of the filament is shown in a 0.5-s exposure. Because of the travelling wave and the inextensibility of the filament, the free end executes a 'figure of eight' trajectory.

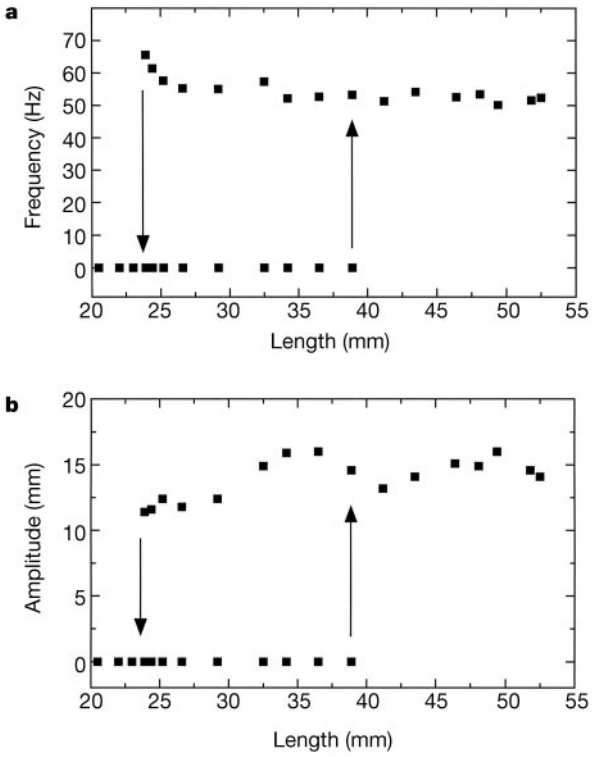

Figure 3 The flapping frequency and amplitude of the filament as functions of L, the filament length. **a**, Flapping frequency; **b**, amplitude. The disturbance level needed for the jump from a steady state to the flapping state decreases with increased filament length, up to a limit where a steady state can no longer survive.

Although the flapping state is stable, the filament can be forced to return to the stretched-straight state by briefly holding straight the filament (such as with a pair of tweezers), or by shortening it until L is brought below L_c. Both stretched-straight and flapping states can be alternately selected, either by externally forcing the filament or by exploiting the dynamical hysteresis.

If L is sufficiently large, the stable stretched-straight state disappears, and only the flapping state remains. It is difficult to determine experimentally whether this is due to a loss of linear stability at some finite L, or is due to finite noise in the flow being sufficient to overcome a barrier between the two stable states. Overall, the observed phenomenon suggests the existence of a sub-critical bifurcation (see ref. 13 for example).

For a very long filament ($L > 6$ cm), the observed flapping motion seems to be limited to within about two wavelengths of the free end. This suggests that the tension exerted on the filament, arising from viscous shear stress exerted by the flowing fluid, as well as from the weight of the filament, constrains the motion; the flapping motion thus becomes an edge effect.

Figure 3 shows the experimental measurements of the flapping amplitude and frequency as functions of the filament length. In the measurements, the free stream flow speed is fixed, and the length of the filament is changed incrementally. The amplitude of the flapping motion, measured as the maximum flapping span, changes with length (Fig 3a). The frequency is essentially constant as a function of length (Fig. 3b).

An important generalization to consider is the dynamics of two 'compliant walls' that interact with each other through the flowing fluid. This is an open-flow analogue to the dynamics of a compliant pipe[14]. When two identical filaments are inserted side by side into the flowing soap film, cooperative dynamical states are observed. As shown in Fig. 4 (fixing $L = 3.6$ cm and $U = 220$ cm s^{-1}), if the inter-filament distance d is sufficiently small ($d/L < 0.21 \pm 0.04$), the filaments tend to phase lock and flap in phase with each other

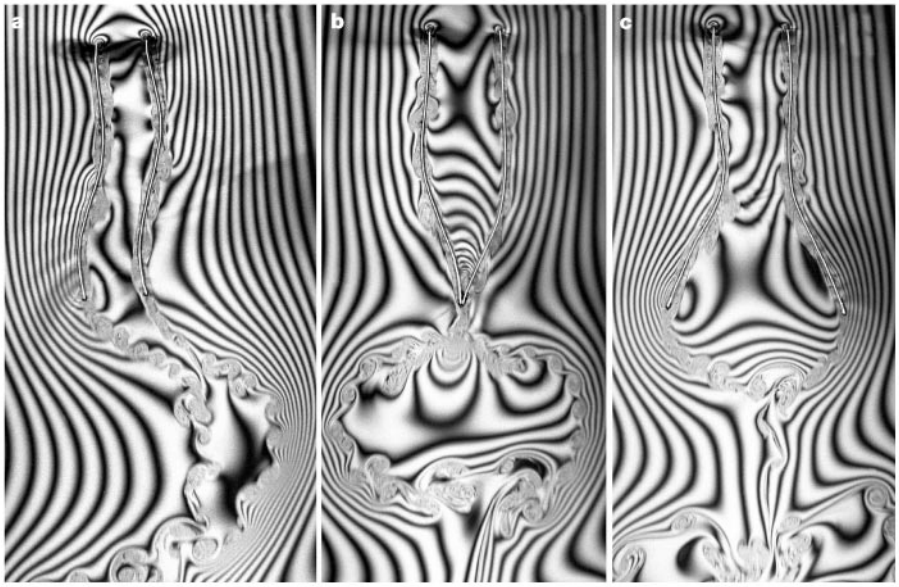

Figure 4 Dual filaments of the same length oscillating at the same frequency, when $L = 3.5$ cm and $U = 220$ cm s^{-1}. **a**, In-phase oscillation, with $d/L = 0.17$; **b** and **c**, out-of-phase oscillations, with $d/L = 0.25$. When two filaments touch, the local instantaneous thickness of the soap film is expected to increase to a dimension comparable to the filament diameter. As opposed to the single-filament case, the soap film is evidently stretched and compressed, as is indicated at places where the interference fringes are almost perpendicular to the flow direction.

(Fig. 4a). As the distance is increased ($d/L > 0.21$), the filaments switch to become locked in an out-of-phase state (Fig. 4b and c) where they flap symmetrically about the centre-line. Stretching and compression of the film is evident from the interference patterns, where many fringes between the filaments are perpendicular to the flow direction. When the tips of both filaments touch each other, the film is significantly compressed. The number of fringes seen in Fig. 4c indicates that the film thickness has increased by at least 3.2 μm. After this point of singularity, the enclosed fluid is released like a droplet and it spreads into the adjacent plane. The out-of-phase (symmetric) flapping state has an approximately 35% higher frequency than the in-phase state. As d is further increased, the coupling between the filaments weakens, and each tends to behave independently of the other. Moreover, filaments can be forced, from any of these states (at least over a modest range of lengths), into being stretched straight. This is the third cooperative state.

Historically, the flapping of sails and flags has interested fluid dynamicists primarily as an apparent indication of the growth of disturbances in a fluid flow. Rayleigh[1] relates the flag to the Kelvin–Helmholtz instability—the instability of an interface between two distinct, parallel streams—in the case where both streams have the same density and far-field velocity. Prandtl[2] discusses the dynamics of the interface as an instance of curvature effects on velocity. At any bulge in the flag the velocity is enhanced on one side and reduced on the other, the flapping being associated therefore with vorticity on the dividing streamline. From either viewpoint the disturbances are owing to vorticity in the neighbourhood of the flag. This vorticity, perhaps shed from an upstream flagpole, tends to be swept downstream with the flow, and its streamwise variations cause ripples in the flag that grow roughly linearly with distance downstream.

The phenomena reported here are not, however, caused by vorticity introduced at a flagpole. They seem instead to be associated with features mostly neglected in the classical descriptions—the filament's tension, elastic rigidity and mass, in addition to the dynamic interaction of the filament with the fluid flow. Indeed, near the transition point to flapping, the mass of the filament has come into balance with the mass of the interacting fluid, while the elastic energy of the filament balances the kinetic energy of the fluid. This is not so for shorter filaments, where the dynamical effect of the fluid flow is relatively lessened. We propose that this balance of effects induces a bifurcation to instability of the stretched-straight state, and leads to the flapping of the filament.

The suspended filament studied here is an open system with similarities to classical aerodynamic flutter (for example, see ref. 15), and to confined flows with compliant boundaries, studied for example in models of blood flow[14,16]. The vorticity shed from the downstream edge introduces a fundamental difference between confined flows and the open finite filament, and the conditions determining the shed vorticity perhaps play an important role in our dynamic problem. The linear stability of a two-dimensional flexible flag has been recently studied theoretically[17], though under strong simplifications, such as the use of a quasi-steady Bernoulli equation that, among other things, neglects vortex shedding and wake vorticity. Whereas this work does predict a bifurcation to instability with increasing filament length, it occurs at much smaller lengths than are observed here.

There are also peculiarities of soap film flows that would not be present in a two-dimensional viscous flow, if such a system could be otherwise realized. For example, to film stretching and compression, a soap film can manifest Marangoni (short-time response) and Gibbs (long-time response) elasticity[18]. However, if present, we expect neither of these resistive responses to provoke an instability, as is apparently observed in the transition from the stretched-straight state. Instead, these elastic responses should help set flapping frequencies and wavelengths, in coordination with the filament stiffness. Moreover, an examination of the interference patterns in the single-filament case shows little evidence of dynamical compression (or stretching) of the film, because the flow is accelerating in those areas where compression is expected. Conversely, film compression and expansion is more evident in the two-filament case (compare Fig. 4b and c), although the detailed effect is as yet unknown.

We observe that the cooperative in- and out-of-phase states in the interacting filament experiments are consistent with the theory for a pair of coupled oscillators considered as two identical "vortex emitters"[19]. There, the strength of the coupling combined with the nonlinearity of the system causes oscillations in two modes with different symmetries. In an earlier work[20,21], the coupling of vortex streets shed from short cylinders were studied experimentally and different symmetries of coupled wakes were observed. In this case, the flow obstacles were solid and immobile.

Swimming offers alternatives comparable to the bistability of our filament. The stretched-straight state is the analogue of a glide, whereas the flapping state is analogous to swimming. Efficient propulsion uses the natural oscillations of the swimmer, which in the filament is a property mediated by stiffness. □

Methods

Set-up of the flowing soap film

Two thin nylon wires (0.3 mm in diameter) separate at a nozzle (0.5 mm inner diameter) attached to the bottom of a reservoir, which contains soapy water maintained at a fixed pressure head. A stopcock regulates the flow rate through the nozzle. The wires extend downwards to a lower container 2.4 m below. The spreading angle of the two wires at the top is about 8.3 degrees. From the interference pattern, the film thickness is seen to vary smoothly across the film by about 20% from its mean. Owing to air drag, a terminal velocity is nearly reached within approximately 60 cm from the nozzle[6]. In air, the velocity profile near the centre is close to being uniform, with velocity differences within 5% of mean, over 65% of the span about the midline. The filament is fixed using a thin tube (0.6 mm in diameter) perpendicular to the soap film. The Reynolds number for the filament is $\mathrm{Re} = UL/\nu$, where U is the upstream flow speed, L the length of the filament and $\nu \approx 0.04\ \mathrm{cm^2\ s^{-1}}$ the kinematic viscosity of the soap film[5].

Velocity measurement

The soap solution is seeded with small polystyrene beads, 2 μm in diameter. A charge-coupled device (CCD) camera records the migration of the beads from frame to frame, when the flow is illuminated with a stroboscope operating at twice the video frequency. Velocity is determined by measuring of displacement of beads from any two successive frames. The accuracy is better than 0.4%. For velocity time series, a laser Doppler velocimeter (Model LDP-100, TSI Inc.) was used.

Flow and filament visualization

The flow is visualized using an interference technique, with a low-pressure sodium lamp as the monochromatic light (589.0 nm and 589.6 nm) illuminating the soap film. Two water–air interfaces of the film render an interference pattern, whose fringes show thickness contours of the film. The thickness variation from bright to bright (or dark to dark) fringes is 0.22 μm. Because the thickness of the film is advected as a passive scalar by the flow field[5], the interference pattern captures the flow pattern qualitatively.

Received 5 May; accepted 16 October 2000.

1. Rayleigh, Lord. On the instability of jets. *Proc. Lond. Math. Soc.* **X,** 4–13 (1879).
2. Prandtl, L. *Essentials of Fluid Mechanics* (Hafner, New York, 1952).
3. Couder, Y., Chomaz, J. M. & Rabaud, M. On the hydrodynamics of soap films. *Physica D* **37,** 384–405 (1989).
4. Gharib, M. & Derango, P. A liquid-film (soap film) tunnel to study two-dimensional laminar and turbulent shear flows. *Physica D* **37,** 406–416 (1989).
5. Martin, B. K. & Wu, X.-L. Shear flow in a two-dimensional Couette cell: A technique for measuring the viscosity of free-standing liquid films. *Rev. Sci. Instrum.* **66,** 5603–5608 (1995).
6. Rutgers, M. A., Wu, X.-L., Bhagavatula, R., Petersen, A. A. & Goldburg, W. I. Two-dimensional velocity profiles and laminar boundary layers in flowing soap films. *Phys. Fluids* **8,** 2847–2854 (1996).
7. Kellay, H., Wu, X-L. & Goldburg, W. I. Experiments with turbulent soap film. *Phys. Rev. Lett.* **74,** 3975–3978 (1995).
8. Tritton, D. J. *Physical Fluid Dynamics* 2nd edn (Oxford Univ. Press, New York, 1988).
9. Bénard, H. Formation de centres de giration à l'arriére d'un obstacle en mouvement. *C. R. Acad. Sci. Paris* **147,** 839–842 (1908).
10. Thorpe, S. A. Experiments on the instability of stratified shear flows: miscible fluids. *J. Fluid Mech.* **46,** 299–319 (1971).
11. Triantafyllou, M. S. & Triantafyllou, G. S. An efficient swimming machine. *Sci. Am.* **272,** 64–70 (1995).
12. Anderson, J. M., Streitlien, K., Barrett, D. S. & Triantafyllou, M. S. Oscillating foils of high propulsive efficiency. *J. Fluid Mech.* **360,** 41–72 (1998).
13. Drazin, P. G. & Reid, W. H. *Hydrodynamic Stability* 374–375 (Cambridge Univ. Press, Cambridge, 1981).
14. Pedley, T. J. *The Fluid Mechanics of the Large Blood Vessels* (Cambridge Univ. Press, Cambridge, 1979).

15. Scanlan, R. H. *Introduction to the Study of Aircraft Vibration and Flutter* (McMillan, New York, 1951).
16. Païdoussis, M. P. *Fluid–Structure Interaction* Vol. I (Academic, San Diego, 1998).
17. Fitt, A. D. & Pope, M. P. The unsteady motion of a two-dimensional flag with bending stiffness. *J. Eng. Sci.* (submitted).
18. Chomaz, J. M. & Cathalau, B. Soap films as two-dimensional classical fluids. *Phys. Rev. A* **41,** 2243–2245 (1990).
19. Lopez-Ruiz, R. & Pomeau, Y. Transition between two oscillation modes. *Phys. Rev. E* **55,** R3820–R3823 (1997).
20. Peschard, I. & Le Gal, P. Coupled wakes of cylinders. *Phys. Rev. Lett.* **77,** 3122–3125 (1996).
21. Peschard, I., Le Gal, P. & Takeda, Y. On the spatio-temporal structure of cylinder wakes. *Exp. Fluids* **26,** 188–196 (1999).

Acknowledgements

We thank L. Becker, A. Belmonte, F. Hayot and C. Wiggins for helpful discussions. We thank D. Havir for assistance with the LDV measurements. This work was supported in part by the National Science Foundation and by the Department of Energy.

Correspondence and requests for materials should be addressed to J.Z. (e-mail: jun@cims.nyu.edu).

Observation of five-fold local symmetry in liquid lead

H. Reichert*, O. Klein*†, H. Dosch*, M. Denk*, V. Honkimäki‡, T. Lippmann§ & G. Reiter‖

* *Max-Planck-Institut für Metallforschung, 70569 Stuttgart, Germany*
‡ *European Synchrotron Radiation Facility ESRF, 38043 Grenoble, France*
§ *Hamburger Synchrotronstrahlungslabor HASYLAB, 22607 Hamburg, Germany*
‖ *Physics Department, University of Houston, Houston, Texas 77204-5506, USA*

The local point symmetry of the short-range order in simple monatomic liquids remains a fundamental open question in condensed-matter science. For more than 40 years it has been conjectured[1–4] that liquids with centrosymmetric interactions may be composed of icosahedral building blocks. But these proposed mobile, randomly orientated structures have remained experimentally inaccessible owing to the unavoidable averaging involved in scattering experiments, which can therefore determine only the isotropic radial distribution function. Here we overcome this limitation by capturing liquid fragments at a solid–liquid interface, and observing the scattering of totally internally reflected (evanescent) X-rays, which are sensitive only to the liquid structure at the interface. Using this method, we observe five-fold local symmetry in liquid lead adjacent to a silicon wall, and obtain an experimental portrait of the icosahedral fragments that are predicted to occur in all close-packed monatomic liquids. By shedding new light on local bond order in disordered structures such as liquids and glasses, these results should lead to a better microscopic understanding of melting, freezing and supercooling.

The crystalline solid state is characterized by a long-range positional order of the atomic density at position $\mathbf{r}$, $\rho_s(\mathbf{r}) = \Sigma_m \delta(\mathbf{r}-\mathbf{R}_m)$, where $\mathbf{R}_m$ denotes the lattice positions of the atoms, and an associated orientational bond order belonging to one of the well-known allowed one-, two-, three-, four- or six-fold crystalline symmetries. In a diffraction experiment, δ-function Bragg reflections

$$S_s(\mathbf{q}) = \int \rho_s(\mathbf{r}) e^{i\mathbf{q}\mathbf{r}} d\mathbf{r} = \sum_{HKL} \delta(\mathbf{q} - \mathbf{G}_{HKL}) \quad (1)$$

that is, 'Laue spots', are observed that show the associated point symmetry of the lattice. Here $\mathbf{q} = \mathbf{k}_f - \mathbf{k}_i$ is the momentum transfer given by the incident and diffracted wavevectors $\mathbf{k}_i$ and $\mathbf{k}_f$, respectively, and $\mathbf{G}_{HKL}$ are the reciprocal lattice vectors). In contrast, the liquid state exhibits short-range order extending only a few atomic distances given by the liquid correlation length ξ, which is typically in the range 3–8 Å in simple liquids. It can in principle be determined from the associated liquid pair correlation function $g_l(r)$. Even simple liquids can be considerably supercooled[5], indicating a pronounced barrier to the transition between the supercooled metastable liquid and the thermodynamically stable solid. This supercooling phenomenon may be understood by assuming that the local liquid correlations have non-crystalline symmetries that have to be broken in the crystallization process. In fact, since the early work by Frank[1], Bernal[2,4] and Scott[3], a number of authors have proposed that the local liquid correlations in monatomic liquids, which exhibit centrosymmetric interactions favouring a close-packed local environment, are composed of defective or fragmented icosahedral building blocks that exhibit a five-fold symmetry[1–4,6–8] (Fig. 1a). As these local liquid correlations are isotropically distributed, a conventional diffraction experiment unavoidably yields a 4π average:

$$S_l(q) = 1 + \rho_o \int [g_l(r) - 1] e^{iqr} dr \quad (2)$$

this permits access only to the pair correlation function $g_l(r)$ of the liquid. Consequently, the intrinsic local liquid symmetry has withstood any experimental access. For a scattering experiment attempting to reveal the local liquid symmetry, a microscopic mechanism has to be provided that is able to capture the liquid building blocks in space and time. Here we show that this can in fact be achieved at solid–liquid interfaces by an appropriate combination of solid and liquid components.

At solid–liquid interfaces, the crystalline potential acts on the adjacent liquid in two ways. (1) Perpendicular to the wall, a liquid density oscillation appears within an interfacial layer of thickness ξ^* (see ref. 9 for a review). This hard-wall-induced packing effect has been observed at various solid–liquid interfaces[10–12] as well as at free metallic liquid surfaces[13,14]. (2) In the lateral direction $\mathbf{r}_\parallel$, the

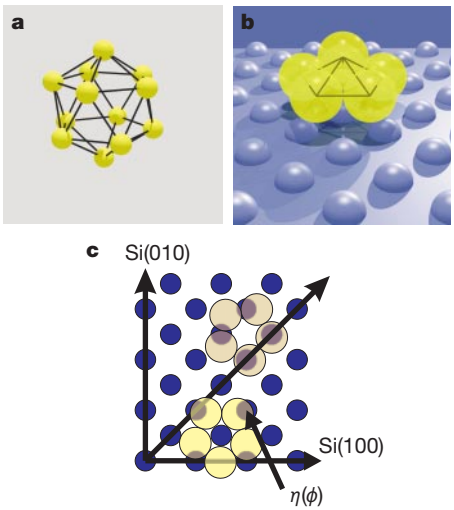

Figure 1 View of the dominant motif in the structure of bulk liquid lead and of interfacial liquid lead. **a**, Polytetrahedral arrangement predicted for close-packed monatomic liquids. **b**, Upper (pentagonal) half of the Pb icosahedron (**a**) captured by the potential landscape of the primitive Si(001) surface. **c**, Projection of the pentagonal structure onto four-fold coordinated sites of the Si(001) surface (lower pentagon, upper site position with minimum overlap of the projected electron density for rotation angle $\phi_n = 2\pi n/20$, where n is an integer; upper pentagon, hollow site with minimum overlap for $\phi_n = 2\pi(n+1/2)/20$; the overlap is denoted by η and shown in Fig. 3c as a function of the rotation ϕ of the pentagon).

† Deceased.